DOI: 10.1002/ejic.200600777

(Pentabenzylcyclopentadienyl)molybdenum Complexes: Synthesis, Structures and Redox Properties

Sónia Namorado,[a] Jinlan Cui,[a] Cristina G. de Azevedo,[a] M. Amélia Lemos,[b] M. Teresa Duarte,[a] José R. Ascenso,[a] Alberto R. Dias,[a] and Ana M. Martins*[a]

Keywords: Molybdenum / Tungsten / Cyclopentadienyl ligands / Half-sandwich complexes / Cyclic voltammetry

[MCpBz(CO)$_3$]$_2$ (M = Mo **3**, W **4**; CpBz = pentabenzylcyclopentadienyl) complexes were prepared by reaction of Li[MCpBz(CO)$_3$] [M = Mo (**1**), W (**2**)] with Fe^{III}. [MoCpBz(CO)$_2$]$_2$ (**5**) can be prepared by thermal elimination of CO from **3** and also by reaction of **1** with C_3H_5Br. The steric bulk of the CpBz ligands causes all the dimers to exist either in the solid state or in solution as the *trans* isomers. The hydrido complexes [MH(CpBz)(CO)$_3$] [M = Mo (**6**), W (**7**)] were prepared by reactions of **1** and **2** with H$^+$. Cyclic voltammetry and controlled potential coulometry of **5** in CH_2Cl_2, thf and CH_3CN were performed and mechanisms for the redox behaviour are proposed.

Introduction

The thermodynamic and kinetic properties of transition metal complexes are strongly dependent on the interplay of the ligands' stereochemical and electronic features. For metallocene complexes, the importance of cyclopentadienyl (Cp) substituents is extensively documented, with current practice being to tune the metal centres' reactivity through the choice of appropriate Cp ligands. In this context, we recently became interested in pentabenzylcyclopentadienyl (CpBz) derivatives with the aim of assessing the influence of the five bulky benzyl groups on the structures and properties of half-sandwich Mo and W complexes. Preliminary studies with [MoCpBz(O)$_2$Cl] have shown an enhanced performance in the catalytic epoxidation of cyclooctene. A comparison of [MoCp′(O)$_2$Cl] (Cp′ = Cp, Cp*, Cp*i*Pr$_4$, CpBz) complexes showed that the CpBz derivative leads to the most active and stable catalyst system when activated with *t*BuOOH.[1] Moreover, chlorination reactions of low oxidation-state (CpBz)carbonylmolybdenum and -tungsten complexes also differ from those of their Cp and Cp* analogues. In particular, the reactions of [MoCpBz(CO)$_3$(CH$_3$)] with PCl$_5$ or PhICl$_2$ have been observed to proceed by different routes leading to the formation of [MoCpBz{η^2-C(O)CH$_3$}Cl$_3$] or [MoCpBzCl$_4$], respectively.[2] Among the extremely varied reactivity of half-sandwich molybdenocene and tungstocene complexes, the application of hydrido complexes of general formula [MCp(CO)$_2$L(H)] (M = Mo, W; L = CO, PR$_3$) as hydrogenation catalysts of ketones and aldehydes has recently been reported.[3,4]

The results presented here are part of our ongoing interest in (pentabenzylcyclopentadienyl)molybdenum and -tungsten reactivity. To determine the influence of the benzyl substituents on the metal electronic features, we performed electrochemical studies of the dimer [MoCpBz(CO)$_2$]$_2$.

Results and Discussion

All new complexes are represented in Scheme 1. Li[MCpBz(CO)$_3$] [M = Mo (**1**), W (**2**)] are readily prepared in thf or dmf solution, respectively, by treating M(CO)$_6$ with LiCpBz.[5] Treatment of **1** and **2** with Fe^{III} in CH_3COOH at 0 °C leads to the formation of [MCpBz(CO)$_3$]$_2$ [M = Mo (**3**), W (**4**)], which precipitate from their solution as red and orange solids, respectively.

The IR spectrum of **3** in KBr pellets shows three bands at 1932, 1901 and 1876 cm^{-1} for the carbonyl ligands. In **4**, the three carbonyl bands appear at 1928, 1897 and 1868 cm^{-1}. These values are lower than those reported for similar [MCp(CO)$_3$]$_2$ complexes (Mo: 1966, 1922, 1914 cm^{-1}; W: 2012, 1952, 1905 cm^{-1}).[6,7]

The ^{1}H NMR spectra of [MCpBz(CO)$_3$]$_2$ in CD_2Cl_2 display only one resonance for the benzyl protons at δ = 3.88 ppm for **3** and δ = 3.92 ppm for **4**. This means that there are no constraints on the free rotation of the pentabenzylcyclopentadienyl ligands around the metal–C$_{5ring}$ and the C$_{5ring}$–CH$_2$Ph bonds and, considering the arrangement of the CpBz ligands in relation to the metal–metal bonds,

---

[a] Centro de Química Estrutural, Instituto Superior Técnico,
Av. Rovisco Pais, 1, 1049-001 Lisboa, Portugal
E-mail: ana.martins@ist.utl.pt
[b] IBB – Institute for Biotechnology and Bioengineering, CEBQ, Instituto Superior Técnico,
Av. Rovisco Pais, 1, 1049-001 Lisboa, Portugal

Supporting information for this article is available on the WWW under http://www.eurjic.org or from the author.

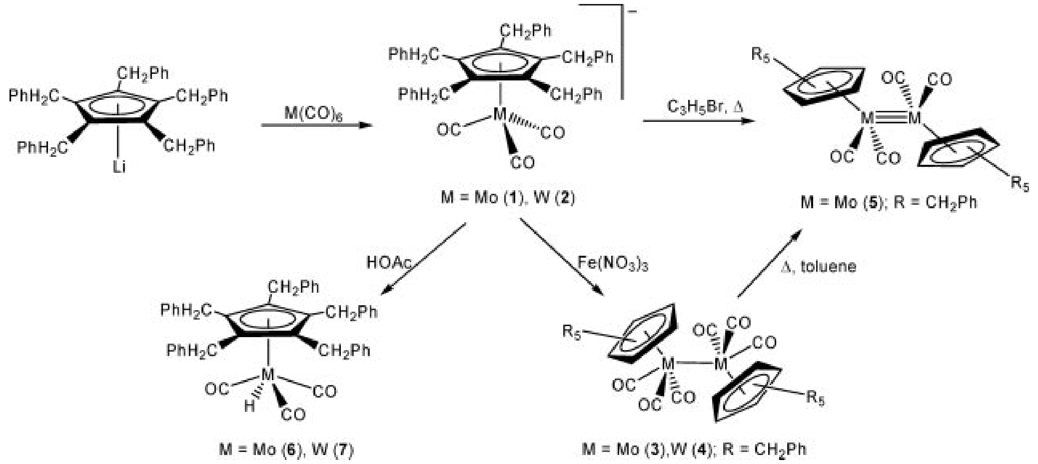

Scheme 1.

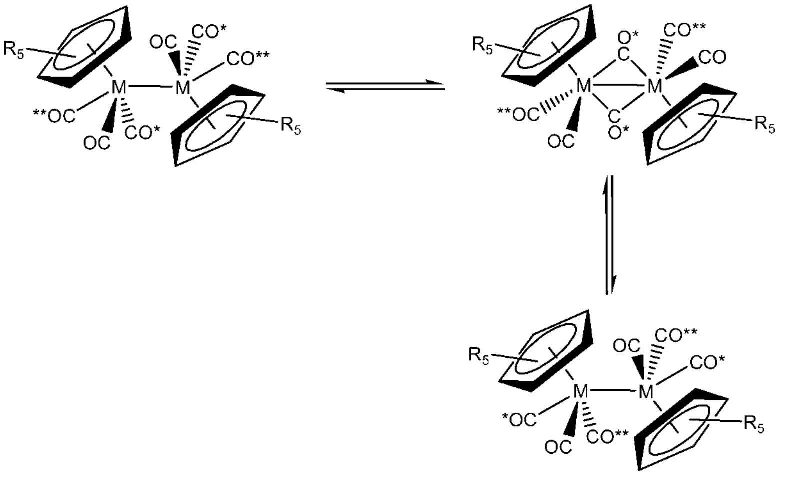

Scheme 2. The asterisks on the CO groups denote inequivalent carbonyl ligands.

is indicative of the presence of only one isomer in solution. The ^{13}C NMR spectra of **3** and **4** corroborate this result and also show that there is a fluxional process in solution that renders the six carbonyl groups equivalent, which gives rise to only one resonance at δ = 234.7 ppm (Mo) and δ = 224.3 ppm (W). The mechanism that accounts for this process is a rapid scrambling of the CO ligands among the six positions available at the two metal centres that involves CO-bridged intermediates, as represented in Scheme 2.[8]

Attempts to block the CO scrambling process by lowering the temperature did not produce any modifications in the NMR spectra down to –80 °C. This behaviour also indicates that *cis*/*trans* isomerisation is not operative, which might be expected on stereochemical arguments, and that the unique isomers in solution are *trans*-[MCpBz(CO)$_3$]$_2$ for both molybdenum and tungsten complexes. Thus, in contrast to their Cp analogues, *cis*/*trans* isomerisation processes in **3** and **4** are hampered.[6,9]

Treatment of Li[MoCpBz(CO)$_3$] with an excess of C_3H_5Br led to the dimer [MoCpBz(CO)$_2$]$_2$ (**5**; Scheme 1). This complex was isolated in 76% yield upon recrystallisation from diethyl ether as orange-red single crystals that were suitable for X-ray diffraction. It is clear that the reaction of C_3H_5Br with **1** is not an elementary process. The formation of [MoCpBz(CO)$_2$]$_2$ probably results from an outer-sphere redox reaction between the anion [MoCpBz(CO)$_3$]$^-$ and C_3H_5Br, leading to the radical [MoCpBz(CO)$_3$], which, upon dimerisation and a thermally induced Mo–CO bond cleavage,[10] finally gives [MoCpBz(CO)$_2$]$_2$. By analogy with the formation of [MoCpBz(CO)$_3$Me] from **1** and MeI, [MoCpBz(CO)$_3$(σ-C_3H_5)] would be the expected product. An allyl radical elimination from the putative Mo^{II} intermediate [MoCpBz(CO)$_3$(σ-C_3H_5)] may, however, be excluded, as it goes against the usual reactivity trend that affords π-allyl coordination by thermal or photochemical activation of σ-allyl precursors.[11,12] The formation of [MoCpBz(CO)$_3$]$_2$ as an intermediate in the synthesis of **5** was confirmed by the quantitative formation of the latter from a toluene solution of **3** under reflux (Scheme 1).

The IR spectrum of **5** shows characteristic peaks due to CpBz and peaks ascribed to the carbonyl ligands at 1878 and 1821 cm^{-1}. These values, which are notably lower than those reported for the Cp (ν_{CO}: 1900 and 1850 cm^{-1}) and

Cp* (ν_{CO}: 1940, 1907, 1874 and 1846 cm^{-1}) analogues,[10,13] should reflect extensive Mo–CO backbonding. The ^{1}H and ^{13}C NMR spectra display one set of CpBz resonances, consistent with the free rotation of the ligand in solution. The magnetically equivalent CO ligands give rise to a resonance at δ = 239.3 ppm.

Li[Mo(CpBz)(CO)$_3$] does not react with other electrophiles like Me$_3$CCH$_2$Br, as attested by the essentially quantitative recovery of the starting material. This result is probably dictated by stereochemical constraints that prevent the coordination of the neopentyl ligand.

The hydrido complexes [MH(CpBz)(CO)$_3$] [M = Mo (**6**), W (**7**)] were obtained upon treatment of **1** with CH$_3$COOH in 90% and 95% yield for **6** and **7**, respectively. The IR spectrum of **6** displays carbonyl stretching vibrations at 2008 (vs), 1928 (vs) and 1822 cm^{-1} (m) and that of **7** shows carbonyl peaks at 2008 (vs) and 1901 cm^{-1} (vs). The lower CO vibration values displayed by **6** and **7** with respect to their Cp and Cp* counterparts are, once more, indicative of a more extensive metal–carbonyl backbonding in the CpBz derivatives.[14,15] The hydrido resonances in **6** appear at δ = –4.85 ppm and in **7** at δ = –6.31 ppm.

Crystals suitable for X-ray analysis of compound **4** were grown from a toluene solution at –20 °C. The molecular structure is shown in Figure 1 and selected bond lengths and angles are listed in Table 1.

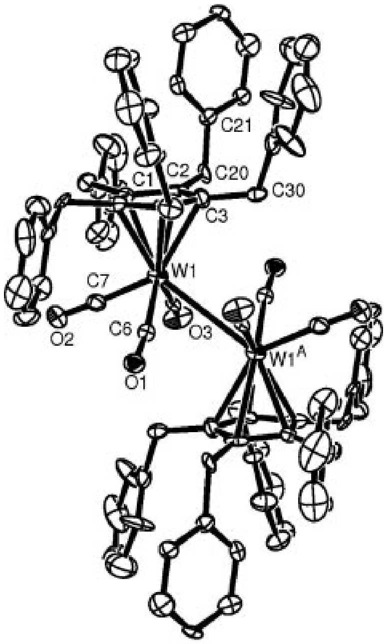

Figure 1. Molecular structure of complex **4**. H atoms have been excluded for clarity. Thermal ellipsoids are shown at the 50% probability level.

Table 1. Selected bond lengths [Å] and bond and torsion angles [°] for **4** and **5**.

	[WCpBz(CO)$_3$]$_2$ (**4**)	[MoCpBz(CO)$_2$]$_2$ (**5**)
M–C(6)	1.976(16)	1.950(3)
M–C(7)	1.913(16)	1.948(3)
M–C(8)	1.992(16)	–
C(6)–O(1)	1.160(16)	1.158(3)
C(7)–O(2)	1.195(16)	1.157(3)
C(8)–O(3)	1.165(17)	–
M–M	3.331(19)	2.5198(8)
M–CpBz(CT)	2.0441(8)	1.9978(6)
M–C(1)	2.342(13)	2.321(3)
M–C(2)	2.402(14)	2.358(2)
M–C(3)	2.427(14)	2.372(3)
M–C(4)	2.387(13)	2.333(2)
M–C(5)	2.349(13)	2.314(2)
C(1)–C(2)	1.424(19)	1.432(3)
C(2)–C(3)	1.49(2)	1.421(4)
C(3)–C(4)	1.410(19)	1.425(3)
C(4)–C(5)	1.46(2)	1.439(4)
C(5)–C(1)	1.401(18)	1.439(3)
M–C(6)–O(1)	171.7(12)	173.1(2)
M–C(7)–O(2)	176.5(12)	171.8(2)
M–C(8)–O(3)	172.6(13)	–
C(6)–M–C(7)	78.1(6)	87.93(11)
C(6)–M–C(8)	110.2(5)	–
C(6)–M–M	67.53(19)	76.58(8)
C(7)–M–C(8)	77.5(6)	–
C(7)–M–M	120.65(19)	71.43(8)
C(8)–M–M	71.62(19)	–
CpBz(CT)–M–C(6)	125.5(4)	116.95(8)
CpBz(CT)–M–C(7)	114.2(4)	119.31(8)
CpBz(CT)–M–C(8)	124.2(4)	–
CpBz(CT)–M–M	125.06(19)	161.54(8)
M–C(1)–C(10)–C(11)	–69.98(19)	–148.2(2)
M–C(2)–C(20)–C(21)	179.45(19)	–162.69(19)
M–C(3)–C(30)–C(31)	–167.43(19)	172.4(2)
M–C(4)–C(40)–C(41)	–161.34(19)	154.8(2)
M–C(5)–C(50)–C(51)	63.41(19)	–176.37(18)

The tungsten coordination geometry is best described as a distorted four-legged piano-stool with a CpBz(CT)–W(1)–W(1A) angle of 125.06(19)° and CpBz(CT)–W(1)–C(n) angles of 125.5(4), 114.2(4) and 124.2(4) for C(6), C(7) and C(8), respectively [CpBz(CT) = centroid of the cyclopentadienyl ring]. The spatial arrangement of the cyclopentadienyl substituents displays three benzyl groups directed opposite to the metal atom and the other two slightly bent towards it. The relative conformation of the phenyl rings is characterised by the torsion angles of the pendent benzyl arms, defined as M–C(CpBz)–C(CH$_2$)–C$_{ipso}$ in Table 1. As a whole, the molecular structure of **4** parallels those previously reported for related dimers.[9,16–19] Two carbonyl ligands of each tungsten atom bend over the metal–metal bond, whereas the remaining carbonyl groups are mutually *trans* in relation to the metal–metal bond and their structural features are typical of linear terminal CO ligands. These carbonyl groups point towards the middle region between the two CpBz benzyl groups that point down towards the tungsten centres. The steric bulk requirements of the CpBz ligands are responsible for elongated metal–metal and metal–CpBz(CT) bond lengths, when compared with analogous complexes [$3.215 < \text{W–W} < 3.287$ Å; $1.995 < \text{W–Cp}'(\text{CT}) < 2.029$ Å].[9,16–19] Short-contact distances have been found between carbonyl oxygen atoms and the methylenic protons of the benzyl groups pointing down and belonging to the other half of the molecule [O(1)···H(20) 2.383, O(3)···H(40) 2.489 Å]. The most peculiar feature of the structure of [WCpBz(CO)$_3$]$_2$ is related to the cyclopentadienyl ring. The C–C bond lengths deserve a comment as two are longer (1.46 and 1.49 Å) than the other three, which are in accordance with the usual average C–C distances in η^5-Cp ligands (1.41 Å).[16] This difference reflects an asymmetry in the metal–ring bonding that is reminiscent of an η^3+η^2 coordination.[20–23]

The molecular structure of [Mo(CpBz)(CO)$_2$]$_2$ is depicted in Figure 2 and some selected distances and angles are listed in Table 1.

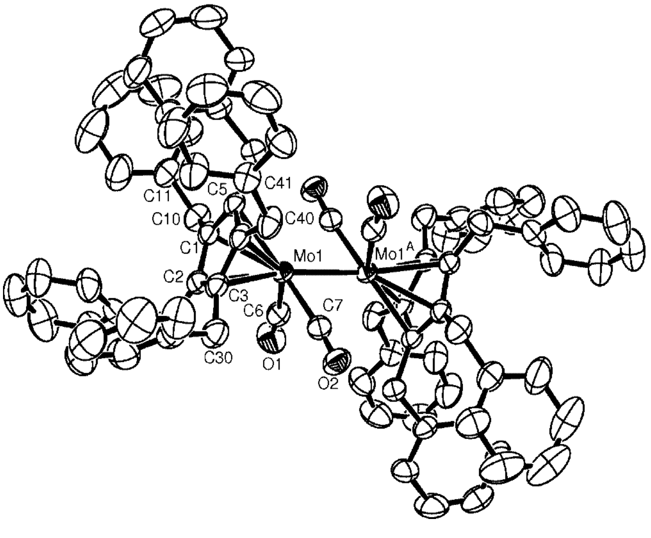

Figure 2. Molecular structure of complex **5**. H atoms have been excluded for clarity. Thermal ellipsoids are shown at the 50% probability level.

The molybdenum coordination is best described as a distorted piano-stool geometry with basal angles ranging between 71.43(8) and 87.93(11)° and CpBz(CT)–Mo(1)–X angles [X = C(6), C(7), Mo(1A)] varying from 116.95(8) to 119.31(8)°. The CpBz(CT)–Mo(1)–Mo(1A) angle [161.54(8)°] is more acute than that reported for [MoCp(CO)$_2$]$_2$, which displays a linear Cp–Mo–Mo arrangement,[13] but close to the values reported for the majority of [MCp′(CO)$_2$]$_2$ complexes [M = Cr, Mo, W; Cp′ = C_5H_5, C_5Me_5, Ind, C_5H_4COOEt, C_5H_3tBu$_2$, $C_5Me_4(CH_2)_2$-NMe$_2$].[13,24–28] The Mo(1)–Mo(1A) distance [2.5198(8) Å] is compatible with a metal–metal triple bond, although it is longer than in [MoCp′(CO)$_2$]$_2$ [Cp′ = C_5H_5 2.448(1) Å, C_5Me_5 2.488(3) Å].[13,28] As generally observed for [MoCp′(CO)$_2$]$_2$ complexes, the carbonyl ligands in **5** are linear semi-bridging.[24,25] The Mo(1)–C(6) [1.950(3) Å] and Mo(1)–C(7) [1.948(3) Å] bond lengths are thus identical to those of similar compounds,[13,25–28] and much shorter than in [MoCp(CO)$_2$]$_2$ [2.14(2) and 2.52(2) Å]. All the CpBz phenyl rings in **5** point away from the metal atom and define torsion angles of between 148.2(2) and 176.37(18)°.

The relative orientation of the cyclopentadienyl rings towards the metal–metal bonds in [Cp′M(CO)$_2$]$_2$ complexes (M = Cr, Mo; Cp′ = C_5H_5, C_5Me_5), which results in linear or bent arrangements, has been attributed to electronic rather than stereochemical reasons. The combination of ring orbitals with σ or π* metal–metal orbitals was taken as the determining factor for the Cp(CT)–M–M angle values whilst pointing out that the metal–ring and metal–metal bonds are strongly interdependent, that is, the Cp rings may be thought of as conjugated with the $M\equiv M$ system.[26] In the case of bent Cp(CT)–M–M arrangements, since σ* metal–metal orbitals are involved, the weakening (and thus the lengthening) of the metal–metal bond is more pronounced.

The molecular structures of **6** and **7** are represented in Figures 3 and 4, respectively, and selected bond lengths and angles are listed in Table 2.

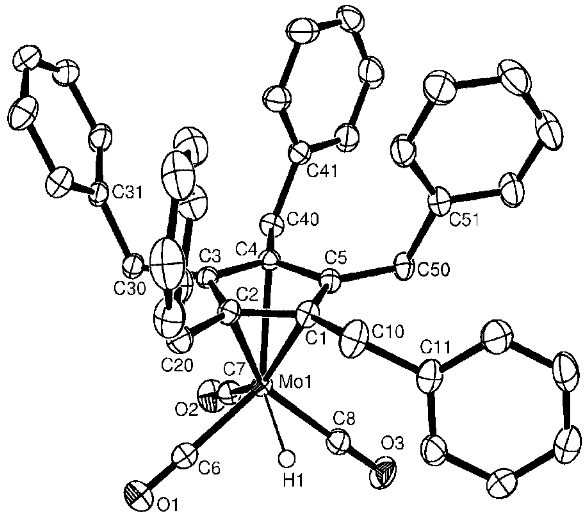

Figure 3. Molecular structure of complex **6**. H atoms have been excluded for clarity, except the hydride ion. Thermal ellipsoids are shown at the 50% probability level.

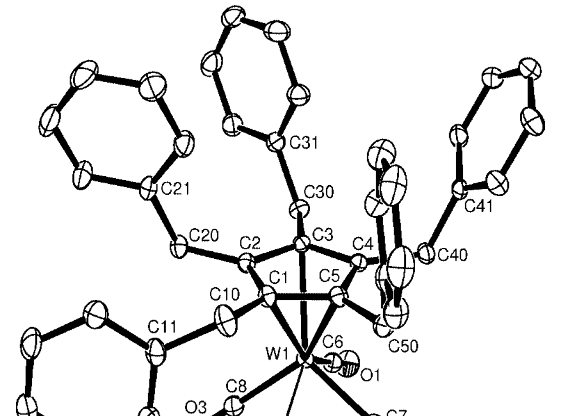

Figure 4. Molecular structure of complex **7**. H atoms have been excluded for clarity, except the hydride ion. Thermal ellipsoids are shown at the 50% probability level.

Table 2. Selected bond lengths [Å] and bond and torsion angles [°] for **6** and **7**.

	[MoH(CpBz)(CO)$_3$] (**6**)	[WH(CpBz)(CO)$_3$] (**7**)
M–C(6)	1.9737(19)	1.9948(15)
M–C(7)	1.9938(18)	1.9771(16)
M–C(8)	1.9815(18)	1.9861(15)
C(6)–O(1)	1.147(2)	1.1522(18)
C(7)–O(2)	1.142(2)	1.1522(19)
C(8)–O(3)	1.146(2)	1.1492(18)
M–H	1.6058(268)	1.7045(216)
M–CpBz(CT)	1.99902(16)	2.00093(11)
M–C(6)–O(1)	175.65(18)	178.82(13)
M–C(7)–O(2)	179.55(17)	175.58(14)
M–C(8)–O(3)	177.44(17)	176.94(14)
C(6)–M–C(7)	81.60(8)	81.14(6)
C(6)–M–C(8)	105.88(7)	81.13(6)
C(7)–M–C(8)	81.74(7)	106.32(6)
CpBz(CT)–M–C(6)	122.85(6)	122.11(4)
CpBz(CT)–M–C(7)	122.19(5)	123.00(5)
CpBz(CT)–M–C(8)	126.94(5)	126.87(4)
CpBz(CT)–M–H	115.91(98)	114.69(72)
M–C(1)–C(10)–C(11)	61.23(22)	–61.65(18)
M–C(2)–C(20)–C(21)	162.94(12)	166.85(9)
M–C(3)–C(30)–C(31)	178.41(11)	159.82(9)
M–C(4)–C(40)–C(41)	–159.78(11)	–178.19(9)
M–C(5)–C(50)–C(51)	–167.15(11)	–163.07(9)

Complexes **6** and **7** have similar four-legged piano-stool metal coordination geometries, as also reported for analogous metal hydride complexes.[29–32] The structural parameters displayed are consistent with the data found in the literature for this class of compounds and will not be discussed further. The M–CpBz(CT)–C(CH$_2$)–C$_{ipso}$ torsion angles are similar to those observed for complex **4**, although in **6** and **7** only one phenyl ring approaches the metal atoms.

Electrochemical Studies

The electrochemical behaviour of [Mo(CpBz)(CO)$_2$]$_2$ (**5**) was investigated by means of cyclic voltammetry (CV) and controlled-potential coulometry (CPC). The CV results in thf, CH$_2$Cl$_2$ and CH$_3$CN, using Bu$_4$NBF$_4$ or Bu$_4$NPF$_6$ as electrolyte, measured at 200 mV s^{-1}, are summarised in Table 3 (Figures S1–S3 in the Supporting Information show the voltammograms of **5** in the three solvents with different electrolytes at different scan rates).

Table 3. Electrochemical data [E_p^{ox}(V) vs. FcH] for **5**.

Solvent	CH$_2$Cl$_2$	THF	CH$_3$CN
Bu$_4$NPF$_6$	0.49	–	0.26 (I) 0.52 (II)
Bu$_4$NBF$_4$	–	0.56	0.26 (I) 0.54 (II)

In thf and CH$_2$Cl$_2$, **5** exhibits one irreversible oxidation process at E_p^{ox} = 0.56 and 0.49 V, respectively (Figure S1, Supporting Information). A different behaviour was observed in CH$_3$CN (Figure 5), where a new irreversible anodic wave appears at a significantly lower oxidation potential of E_p^{ox}(I) = 0.26 V. A second oxidation process occurs in CH$_3$CN at E_p^{ox}(II) = 0.52 V or E_p^{ox}(II) = 0.54 V, depending on the electrolyte. The relative intensity of the two waves varies with the scan rates. Thus, the ratio between the intensity of the second and first oxidation waves increases when the scan rate decreases from 200 to 20 mV s^{-1} (Figure S2, Supporting Information). This behaviour suggests that the oxidation process taking place at the higher potential is related to the product formed at the first oxidation potential by an ECE-type mechanism (ECE = heterogeneous electron transfer, homogeneous chemical reaction and heterogeneous electron transfer, in sequence). Furthermore, the second wave is much higher when Bu$_4$NPF$_6$ is used instead of Bu$_4$NBF$_4$ (Figure S3, Supporting Information). This dependence on the electrolyte is suggestive of a chemical reaction that requires its participation and, assuming that the two oxidation waves are linked by an ECE-type mechanism, the rate of the intermediate chemical reaction must be much higher in the case of PF$_6^-$ than in the case of BF$_4^-$. Moreover, the lower potential at which the first redox process occurs in CH$_3$CN, in comparison with the other solvents, indicates that the first oxidation process should be supported somehow by the solvent.

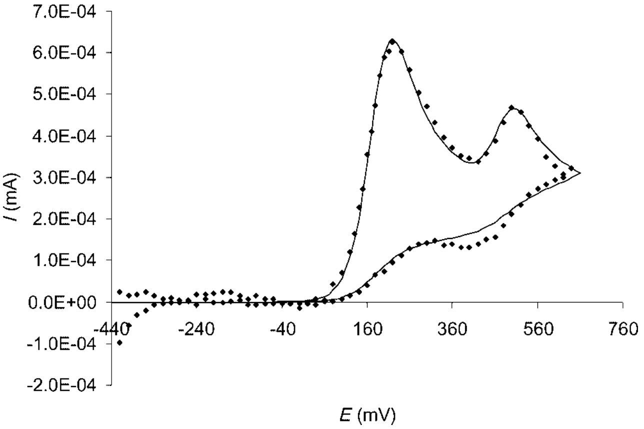

Figure 5. Voltammogram of a solution of **5**, at a Pt disc electrode, at a scan rate of 20 mV s^{-1} in CH$_3$CN with Bu$_4$NBF$_4$ as supporting electrolyte. The line corresponds to simulation using Scheme 3 with the parameters shown in Table 4.

Controlled-potential coulometry of **5** in Bu$_4$NPF$_6$/CH$_2$Cl$_2$, at a potential of 0.56 V, reveals a complex pattern of current vs. time (Figure S5, Supporting Information) that is compatible with the concomitant occurrence of a redox process involving the exchange of four electrons per molecule and a chemical reaction. On the other hand, coulometry of **5** in CH$_3$CN, performed at the first wave potential (0.26 V), reveals an exchange of two electrons independently of the electrolyte used (Figure S4, Supporting Information).

The experimental results described above may be interpreted as follows. The much lower potential observed for the transfer of the first two electrons in CH$_3$CN suggests the participation of the solvent, which, as it is a better donor than CH$_2$Cl$_2$ and thf, makes the metal centre more electron-rich. Based on literature reports, it would be plausible to consider acetonitrile coordination to **5**, leading to the formation of an adduct. This type of compound has been described by Curtis et al., who have reported the addition of soft nucleophiles to $[MoCp(CO)_2]_2$ to give products in which the metal–metal π bonds have been displaced.[33] On the other hand, studies on the oxidation of $[MoCp(CO)_3]_2$ and $[MoCp(CO)_3]^-$ have shown that the cleavage of the dimer occurs with CH_3CN coordination to afford the 19-electron species $[MoCp(CO)_3(CH_3CN)]^{\cdot}$, which are oxidized to $[MoCp(CO)_3(CH_3CN)]^+$ at a lower potential than would be observed for non-stabilized 17-electron species.[34–36] However, efforts to identify a solvent adduct by NMR and IR spectroscopy have proved unsuccessful, and the nature of the interaction with the solvent remains unclear, although it is probable that the oxidation of **5** results in metal–metal bond cleavage and the formation of the cation $[MoCpBz(CO)_2(CH_3CN)_2]^+$.

The intensity of the second oxidation wave observed in CH_3CN depends on the electrolyte counterion. Thus, it is likely that, despite the high dielectric constant of the solvent, ion pairs are formed between the cation $[MoCpBz(CO)_2(CH_3CN)_2]^+$ and the anions BF_4^- or PF_6^-, which are present in a large excess in solution. The rate of formation of these species, which are oxidized at the higher potentials (0.52 or 0.54 V), is reflected in the different peaks' intensity (Figure S3, Supporting Information). Considering the molar amount of **5**, the number of electrons involved in this process is two, which corresponds to one electron per molybdenum centre.

In CH_2Cl_2 and thf a global transfer of four electrons occurs at a unique potential (0.54 or 0.56 V). Taking into consideration this higher potential, it can be assumed that the first oxidation process is not assisted by solvent coordination. This assumption is consistent with the poorer donor ability of these solvents in comparison with CH_3CN. The oxidative cleavage of the metal–metal bond would afford 2 equiv. of $[MoCpBz(CO)_2(L)_2]^+$ (L = CH_2Cl_2, thf). At this potential, two electrons are exchanged in succession. As proposed to occur in CH_3CN, ion-pair formation and subsequent oxidation attest for the exchange of the remaining two electrons of the overall transfer. Ruiz et al. have reported that the two-electron oxidation of $[M_2Cp_2(CO)_4(\mu\text{-}PPh_2CH_2PPh_2)]$ (M = Mo, W) with $[FeCp_2]X$ (X = BF_4, PF_6) is followed by reactions with the counterions, which lead to different reaction pathways.[37] Further support for this interpretation is provided by Bullock and co-workers, who reported the formation of $M\text{–}FBF_3$ complexes in their mechanistic studies of hydride-transfer reactions of transition metal hydrides,[38] and by our own results on the analogous CpBz systems for which $[MoCpBz(CO)_3(CH_2Cl_2)]^+$ and $[MoCpBz(CO)_3(FBF_3)]$ have been identified and by the CV of $[MoCpBz(CO)_3(FBF_3)]$ in NBu_4BF_4/THF, which shows an irreversible anodic wave at 0.54 V.[39]

Simulation of the controlled-potential coulometry results in CH_2Cl_2 and CH_3CN and of the voltammograms obtained in CH_3CN, using Bu_4NBF_4 as electrolyte, has been performed according to Scheme 3. The fittings obtained for the potential coulometry results are presented in the Supporting Information (Figures S4 and S5) and the estimated kinetic parameters in Bu_4NBF_4/CH_3CN are listed in Table 4. Figures 5 and S6 (Supporting Information) depict the fittings obtained for this system at three different scan rates.

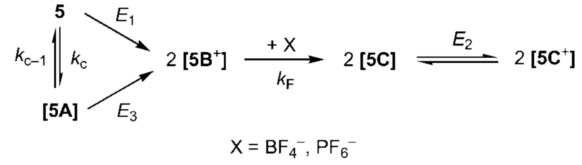

Scheme 3.

Table 4. Kinetic rate constants for the electrochemical behaviour of **5** in Bu_4NBF_4/CH_3CN, at a Pt disc electrode, based on Scheme 3.

Electron transfer	Heterogeneous standard rate constant k_{het} [cm s^{-1}]	Formal potential $E^{0\prime}$ [V]	Transfer coefficient α
E_1	1×10^{-2}	0.38	0.5
E_2	1×10^{-2}	0.49	0.5
E_3	1×10^{-2}	0.23	0.5
Homogeneous rate constants [s^{-1}]			
k_{c1}	2	k_{c-1}	0.2
k_F	5.8		

The first issue to be addressed is the difference in behaviour between the voltammograms obtained in CH_3CN and those displayed in CH_2Cl_2 and thf. It is clear that the performance in the two latter solvents is similar, thus indicating that a series of electron transfers occurs, followed by some sort of chemical reaction that generates a non-electroactive species since the oxidation wave is irreversible for all scan rates studied. Although the second wave in CH_3CN is significantly coincident with the wave observed in the other two solvents, another wave at lower potential is observed. The best fittings of the simulation to the experimental results obtained in CH_3CN require the acceptance of an equilibrium that converts complex **5** into a new species (**5A**) that undergoes oxidation in the first wave. As discussed above, this species should result from an unidentified interaction with the solvent. The apparent first-order rate constant (the solvent concentration is incorporated in the rate constant value) was estimated as $k_{c1} = 2\ s^{-1}$, a much lower value than those found for the coordination of acetonitrile to the $[CpMo(CO)_3]^{\cdot}$ radical[35] (ranging from 6.3×10^5 to $6.0\times10^8\ s^{-1}$) and to the iron centre in $[Fe(\eta^5\text{-}C_6H_7)(CO)_3]^{+}$[40] ($8.0\times10^2\ s^{-1}$). This first wave involves the sequential exchange of two electrons. It was simulated by an ECE sequence and a homogeneous rate constant for the chemical step in-between the two electron-transfer processes of more than 500 s^{-1} was estimated. In CH_2Cl_2 and thf, although it is likely that a similar ECE pattern involving the transfer of two electrons is taking place, the available data is not good enough to estimate the rate constant for the chemical step. However, due to the shape of the voltammetric wave, it is not possible to consider that the two electrons are exchanged in a single step.

The voltammograms obtained in CH_3CN also reveal some additional aspects. During the voltammetric experiment, if the scan rate is sufficiently low, all **5A** is oxidised and, during this period, the equilibrium between **5** and **5A** is displaced towards the latter, which is oxidised in a typical CE mechanism (CE = homogeneous chemical reaction preceding heterogeneous electron transfer). At higher scan rates this interconversion has no time to occur and thus, after oxidation of the initial amount of **5A** present, compound **5** is oxidised at the second wave in the same way as in dichloromethane or thf. This explains why the second wave does not disappear, although it remains relatively small, even at very high scan rates. This second wave has, then, two components that result from the oxidation of **5** and from the oxidation of the ion pair formed by the interaction with the electrolyte counterions, as explained above.

The simulation of the voltammograms obtained in Bu_4NPF_6/CH_3CN may be explained using the same set of parameters listed in Table 4, with the exception of the reaction rate constant for the anion. In this case the value obtained is $k_F = 30\ s^{-1}$, which is significantly higher than that obtained in Bu_4NBF_4/CH_3CN (only $5.8\ s^{-1}$). The cationic species $\mathbf{5B}^+$ and $\mathbf{5C}^+$ are considered to decompose through a first-order chemical reaction with estimated constants of $k_{d1} = 12$ and $k_{d2} = 1.5\ s^{-1}$ (Bu_4NBF_4/CH_3CN) and $k_{d2} = 10\ s^{-1}$ (Bu_4NPF_6/CH_3CN). The simulation results are depicted in Figures 5 and S6 (see Supporting Information).

Previous electrochemical studies on related carbonyl group 6 metal dimers have been dominated by complexes of general formula $[MCp'(CO)_3]_2$, where Cp′ = Cp,[41–43] Cp*,[44] CpR (CpR = η^5-C_5H_4R),[41,45] Fv [Fv = (η^5:η^5-$C_5H_4)_2$][45,46] and M = Mo and W. Even though the electron-transfer processes in the hexacarbonyl dimers involve the disruption of the dinuclear unit,[35,41–43,45,46] as proposed for **5**, and the anodic wave at around 0.5 V compares well with those reported for $[MoCp'(CO)_3]_2$, the cathodic shift observed for the first oxidation wave at 0.26 V in CH_3CN has no parallel in the hexacarbonyl dimers' oxidation, and the irreversibility of the redox process for **5** contrasts with the reversible processes reported for $[MoCp'(CO)_3]_2$.

Conclusion

As a final comment, we conclude that the set of reactions depicted in Scheme 3 explains all the available CV and CPC data, as can be seen from the good fittings obtained at several scan rates. It should be noted, however, that, although this may not be the only possible combination of reaction steps, it is probably the simplest one that fulfils all the experimental observations in agreement with the reported studies found in the literature for analogous systems.

Experimental Section

General Procedures and Starting Materials: All manipulations were carried out under dry nitrogen using standard Schlenk techniques. Solvents were dried and distilled by the usual methods prior to use. Deuteriated solvents were dried with molecular sieves (4 Å), degassed and stored under nitrogen. NMR spectra were recorded at room temperature with a Varian Unity 300 and referenced to the proton and carbon resonances of the residual protonated solvents. Infrared spectra were obtained with a Perkin–Elmer 577 spectrophotometer. Elemental analyses were performed by the Laboratório de Análises do I.S.T., Lisbon, with a Fisons Instruments 1108. The compound HCpBz was prepared according to the described procedure.[5] All other reagents were of commercial grade and used without further purification, except Bu_4NBF_4 and Bu_4NPF_6, which were of electrochemical grade.

[Mo(CpBz)(CO)$_3$]$_2$: HCpBz (1.01 g, 1.96 mmol) was dissolved in thf (20 mL) and a 1.6 M solution of BuLi in hexanes (1.30 mL, 2.08 mmol) was slowly added at –5 °C. The resulting light-yellow solution was stirred for 1 h and then added to a suspension of $Mo(CO)_6$ (0.88 g, 3.34 mmol) in thf (10 mL) and the yellow solution obtained was refluxed overnight. The red mixture formed was cooled to room temperature and a solution of $Fe(NO_3)_3\cdot 9H_2O$ (3.00 g) and acetic acid (2 mL) in water (10 mL) was added dropwise. By the end of the addition, a red precipitate had formed and the mixture was stirred at –5 °C for 2 h. The solution was filtered off and the red precipitate was washed with diethyl ether (10 mL). Yield: 95% (1.29 g, 0.93 mmol). ^1H NMR (CD_2Cl_2, 25 °C): δ = 7.03–6.89 (m, 15 H, *p*-C_6H_5, *m*-C_6H_5), 6.78–6.71 (m, 10 H, *o*-C_6H_5), 3.88 (s, 10 H, C*H*$_2$Ph) ppm. $^{13}C\{^1H\}$ NMR (CD_2Cl_2, –80 °C): δ = 234.7 (*C*O), 138.6 (*i*-C_6H_5), 128.1 (*o*-C_6H_5), 127.7 (*m*-C_6H_5), 125.6 (*p*-C_6H_5), 109.5 [*C*$_5$($CH_2Ph)_5$], 31.3 (*C*H$_2$Ph) ppm. IR (KBr pellet): $\nu_{C\equiv O}$ = 1932, 1901, 1876 cm^{-1}. $C_{86}H_{70}Mo_2O_6$ (1391.4): calcd. C 74.24, H 5.07; found C 74.13, H 5.35.

[WCpBz(CO)$_3$]$_2$: HCpBz (1.07 g, 2.07 mmol) was dissolved in thf (25 mL) and a 1.6 M solution of BuLi in hexanes (1.30 mL, 2.08 mmol) was slowly added at –5 °C. The resulting light yellow solution was stirred for 1 h and was then added to a suspension of $W(CO)_6$ (0.78 g, 2.19 mmol) in thf (10 mL). The yellow solution obtained was refluxed overnight and then cooled to room temperature. A solution of $Fe(NO_3)_3\cdot 9H_2O$ (3.55 g) and acetic acid (2 mL) in water (10 mL) was added dropwise at –10 °C. The mixture was stirred for 3 h and a precipitate formed. The solution was filtered off and the precipitate washed with diethyl ether (10 mL). The orange solid obtained was separated by filtration and dried. Yield: 31% (0.50 g, 0.32 mmol). Crystals suitable for X-ray diffraction were obtained from a toluene solution. ^1H NMR (CD_2Cl_2, 25 °C): δ = 7.01–6.99 (m, 15 H, *p*-C_6H_5, *m*-C_6H_5), 6.71–6.70 (m, 10 H, *o*-C_6H_5), 3.92 (s, 10 H, C*H*$_2$Ph) ppm. $^{13}C\{^1H\}$ NMR (CD_2Cl_2, 25 °C): δ = 224.3 (*C*O), 139.3 (*i*-C_6H_5), 129.3 (*o*-C_6H_5), 128.4 (*m*-C_6H_5), 126.5 (*p*-C_6H_5), 109.2 [*C*$_5$($CH_2Ph)_5$], 32.8 (*C*H$_2$Ph) ppm. IR (KBr pellet): $\nu_{C\equiv O}$ = 1928, 1897, 1868 cm^{-1}. $C_{86}H_{70}O_6W_2$ (1567.2): calcd. C 65.91, H 4.50; found C 65.89, H 4.76.

[MoCpBz(CO)$_2$]$_2$: A solution of Li[MoCpBz(CO)$_3$] (1.81 g, 2.57 mmol) in thf was treated with CH_2=$CHCH_2Br$ (0.27 mL, 3.08 mmol) and heated overnight at 50 °C, whereupon the initial red-brown solution turned red. The volatiles were removed in vacuo to give an oily material, which was extracted with Et_2O. The solution was concentrated and cooled to –20 °C, which led to the formation of orange-red crystals in 76% yield (1.30 g, 0.97 mmol). In an alternative procedure, $[Mo(CpBz)(CO)_3]_2$ (1.76 g, 1.26 mmol) was refluxed overnight in toluene (40 mL) and the solution was then cooled to room temperature and filtered. Solvent removal afforded a red microcrystalline solid in 91% yield (1.54 g, 1.15 mmol). ^1H NMR (C_6D_6): δ = 6.85–6.84 (m, 15 H, *p*-C_6H_5, *m*-C_6H_5), 6.70–6.69 (m, 10 H, *o*-C_6H_5), 4.16 (s, 10 H, C*H*$_2$ Ph) ppm.

$^{13}C\{^1H\}$ NMR (C_6D_6, 25 °C): δ = 239.3 (*C*O), 139.4 (*i*-C_6H_5), 129.3 (*o*-C_6H_5), 128.3 (*m*-C_6H_5), 126.3 (*p*-C_6H_5), 109.3 [$C_5(CH_2Ph)_5$], 32.2 (CH_2Ph) ppm. ^1H NMR ($CDCl_3$): δ = 6.95–6.92 (m, 15 H, *p*-C_6H_5, *m*-C_6H_5), 6.63–6.60 (m, 10 H, *o*-C_6H_5), 3.87 (s, 10 H, CH_2Ph) ppm. $^{13}C\{^1H\}$ NMR ($CDCl_3$, 25 °C): δ = 238.6 (*C*O), 138.9 (*i*-C_6H_5), 128.8 (*o*-C_6H_5), 128.0 (*m*-C_6H_5), 126.0 (*p*-C_6H_5), 108.6 ($C_5\{CH_2Ph\}_5$), 31.5 (CH_2Ph) ppm. IR (KBr pellet): $\nu_{C\equiv O}$ = 1878 (s), 1821 (s) cm^{-1}. $C_{84}H_{70}Mo_2O_4$ (1335.3): calcd. C 75.55, H 5.28; found C 75.05, H 5.44.

[MoH(CpBz)(CO)$_3$]: A 1.6 M solution of BuLi in hexanes (1.4 mL, 2.24 mmol) was added dropwise, at –5 °C, to a solution of HCpBz (1.10 g, 2.13 mmol) in thf (25 mL). The reaction mixture was stirred for 1 h and added to a suspension of [$Mo(CO)_6$] (0.68 g, 2.57 mmol) in thf (10 mL) and the mixture was refluxed for 24 h. After cooling to room temperature, glacial acetic acid (1 mL; 11 mmol) was added and the solution was stirred for 12 h. The solvent was removed under vacuum and the brown solid obtained extracted with diethyl ether and filtered. Concentration and cooling to 4 °C yielded yellow crystals. Yield: 98% (1.47 g). ^1H NMR ([D$_8$]toluene): δ = 6.90 (m, 15 H, *p*-C_6H_5, *m*-C_6H_5), 6.72 (m, 10 H, *o*-C_6H_5), 3.66 (s, 10 H, CH_2Ph), –4.85 (s, 1 H, Mo-*H*) ppm. $^{13}C\{^1H\}$ NMR ([D$_8$]toluene): δ = 228.5 (*C*O), 140.1 (*i*-C_6H_5), 128.9 (*o*-C_6H_5), 128.3 (*m*-C_6H_5), 126.4 (*p*-C_6H_5), 111.4 [$C_5(CH_2Ph)_5$], 32.6 (CH_2Ph) ppm. IR (KBr pellet): $\nu_{C\equiv O}$ = 2008 (s), 1928 (s) cm^{-1}. $C_{43}H_{36}MoO_3$ (696.7): calcd. C 74.13, H 5.21; found C 74.11, H 5.82.

[WH(CpBz)(CO)$_3$]: A 1.6 M solution of BuLi in hexanes (1.2 mL; 1.92 mmol) was added dropwise, at –5 °C, to a solution of HCpBz (1.00 g, 1.94 mmol) in thf (20 mL). The reaction mixture was then stirred for 1 h and the solvent was removed. After the addition of dmf (20 mL), the resulting solution was added to a suspension of [$W(CO)_6$] (0.71 g, 2.00 mmol) in dmf (10 mL). The mixture was then heated at 80 °C for 24 h and cooled to room temperature. Glacial acetic acid (1 mL, 11 mmol) was then added and the solution stirred overnight. The volatiles were removed under vacuum and the brown solid obtained extracted with diethyl ether to give a yellowish solution, which was filtered and the solvents were evaporated to dryness. Yield: 95% (1.47 g). ^1H NMR ([D$_8$]toluene): δ = 6.88 (m, 15 H, *p*-C_6H_5, *m*-C_6H_5), 6.68 (m, 10 H, *o*-C_6H_5), 3.69 (s, 10 H, CH_2Ph), –6.31 (s, 1 H, W-*H*) ppm. $^{13}C\{^1H\}$ NMR ([D$_8$]toluene): δ = 219.4 (*C*O), 139.9 (*i*-C_6H_5), 128.9 (*o*-C_6H_5), 128.3 (*m*-C_6H_5), 126.5 (*p*-C_6H_5), 109.9 [$C_5(CH_2Ph)_5$], 32.7 (CH_2Ph) ppm. IR (KBr pellet): $\nu_{C\equiv O}$ = 2008 (s), 1901 (s) cm^{-1}. $C_{43}H_{36}O_3W$ (784.6): calcd. C 65.82, H 4.62; found C 65.92, H 4.80.

General Procedures for X-ray Crystallography: Pertinent details for the individual compounds can be found in Tables 5 and 6. Crystallographic data for compounds **4**, **6** and **7** were collected using graphite-monochromated Mo-K_α radiation (λ = 0.71069 Å) with a Bruker AXS-KAPPA APEX II area detector diffractometer equipped with an Oxford Cryosystem open-flow nitrogen cryostat; data were collected at 150 K for compounds **4** and **6** and at 130 K for compound **7**. Cell parameters were retrieved using the Bruker

Table 5. Crystallographic data for **4** and **5**.

	4	**5**
Empirical formula	$C_{86}H_{70}O_6W_2$	$C_{84}H_{68}Mo_2O_4$
Formula mass	1567.12	1335.28
Temperature [K]	130(2)	293(2)
Wavelength [Å]	0.71069	0.71069
Crystal system	triclinic	monoclinic
Space group	$P\bar{1}$	$P2_1/c$
a [Å]	12.131(3)	11.322(5)
b [Å]	12.154(2)	13.817(5)
c [Å]	12.587(3)	21.630(7)
α [°]	86.157(9)	90
β [°]	79.061(10)	102.36(2)
γ [°]	63.143(9)	90
Volume [Å^3]	1625.2(7)	3305(2)
Z	2 (half molecule)	4 (half molecule)
$D_{calcd.}$ [g cm^{-3}]	1.601	1.342
Absorption coefficient	3.595 mm^{-1}	0.432 mm^{-1}
F(000)	782	1380
Crystal size [mm]	0.2 × 0.2 × 0.2	–
Crystal morphology	cube	needle
Colour	orange	red
θ range for data collection [°]	1.9–24.2	1.76–25.99
Limiting indices	$-12 \le h \le 12$ $-12 \le k \le 12$ $-12 \le l \le 13$	$0 \le h \le 13$ $0 \le k \le 17$ $-26 \le l \le 26$
Reflections collected/unique	9012/3749 [*R*(int) = 0.1110]	6779/6442 [*R*(int) = 0.0231]
Completeness to θ	71.9% (θ = 24.2°)	99.4% (θ = 25.99°)
Refinement method	full-matrix least-squares on F^2	
Data/restraints/parameters	3749/6/355	6442/0/406
Goodness of fit on F^2	1.020	1.017
Final *R* indices [$I > 2\sigma(I)$]	$R1 = 0.0780$, $wR2 = 0.1796$	$R1 = 0.0340$, $wR2 = 0.0787$
R indices (all data)	$R1 = 0.1224$, $wR2 = 0.2087$	$R1 = 0.0564$, $wR2 = 0.0856$
Extinct. coefficient	0.0133(2)	none
Absorption correction	multiscan	none
Largest difference peak/hole [e Å^{-3}]	3.75/–3.59	0.526/–0.491

Table 6. Crystallographic data for **6** and **7**.

	6	**7**
Empirical formula	$C_{43}H_{36}MoO_3$	$C_{43}H_{36}O_3W$
Formula mass	696.66	784.57
Temperature [K]	150(2)	130(2)
Wavelength [Å]	0.71069	0.71069
Crystal system	monoclinic	monoclinic
Space group	$P2_1/n$	$P2_1/n$
a [Å]	13.1690(9)	13.1880(9)
b [Å]	15.2930(10)	15.2970(10)
c [Å]	16.9420(10)	16.9500(12)
β [°]	95.396(3)	95.302(3)
Volume [$Å^3$]	3396.9(4)	3404.8(4)
Z	4	4
$D_{calcd.}$ [$g\,cm^{-3}$]	1.362	1.531
Absorption coefficient	0.426 mm^{-1}	3.432 mm^{-1}
$F(000)$	1440	1568
Crystal size [mm]	0.40 × 0.20 × 0.05	0.20 × 0.10 × 0.10
Crystal morphology	prism	prism
Colour	yellow	yellow
θ range for data collection [°]	1.80–30.49	1.80–39.94
Limiting indices	$-18 \le h \le 18$ $-21 \le k \le 21$ $-24 \le l \le 24$	$-23 \le h \le 23$ $-24 \le k \le 27$ $-30 \le l \le 28$
Reflections collected/unique	94559/10331 [R(int) = 0.0620]	101111/20943 [R(int) = 0.0366]
Completeness to θ	99.7%	99.6%
Refinement method	full-matrix least-squares on F^2	
Data/restraints/parameters	10331/0/428	20943/0/428
Goodness of fit on F^2	1.088	1.018
Final R indices [$I > 2\sigma(I)$]	$R1 = 0.0303$, $wR2 = 0.0814$	$R1 = 0.0285$, $wR2 = 0.0595$
R indices (all data)	$R1 = 0.0472$, $wR2 = 0.0950$	$R1 = 0.0506$, $wR2 = 0.0667$
Absorption correction	none	none
Largest difference peak/hole [$e\,Å^{-3}$]	0.447/–0.417	1.062/–0.903

SMART software and refined using SAINT with all observed reflections. Absorption corrections were applied using SADABS. Data for compound **5** were collected at room temperature with a MACH3-Bruker Nonius diffractometer equipped with an Mo-K_α radiation ($\lambda = 0.71069$ Å) source. Data were corrected for Lorentz and polarisation effects but not for absorption. Cell dimensions were determined from the setting angles of 25 reflections, within θ values of 15–17°. The structures were solved by direct methods using either SHELXS-97[47] or SIR 97[48] and refined using full-matrix least-squares refinement against F^2 using SHELXL-97.[47] All programs are included in the package of programs WINGX, version 1.64.05.[49] All non-hydrogen atoms were refined anisotropically and all hydrogen atoms except the hydride ions were inserted in idealised positions and allowed to refine as riding on the parent carbon atom. The molecular structures were produced with ORTEP3 for Windows,[50] included in the software package. CCDC-616390, -617703, -616388 and -616389 for complexes **4**, **5**, **6** and **7**, respectively, contain the supplementary crystallographic data for this paper. These data can be obtained free of charge from The Cambridge Crystallographic Data Centre via www.ccdc.cam.ac.uk/data_request/cif.

General Procedures for Electrochemistry: Cyclic voltammetric and controlled-potential coulometry measurements were carried out using a Radiometer DEA 101 Digital Electrochemical Analyser interfaced with an IMT 102 Electrochemical Interface. For cyclic voltammetry measurements, a three-electrode cell with a total volume of around 5 mL was used. A platinum disc electrode was used as working electrode, the counter-electrode was a Pt wire and a silver wire was used as a pseudo-reference electrode; this electrode was kept in a separate compartment and connected to the main compartment by a Luggin capillary. The ferrocene/ferrocenium couple was used as internal standard to measure wave potentials, according to IUPAC recommendations.[51] The controlled-potential coulometry electrochemical cell had a three-compartment design. A large platinum gauze electrode was employed as working electrode, the pseudo-reference electrode was similar to the one used for cyclic voltammetry measurements and it was also connected to the main compartment by a Luggin capillary. The counter electrode was also a platinum gauze electrode and it was kept in a different compartment which was connected to the main compartment by a sintered-glass separation disk. Concentrations of around 0.2 M were used for cyclic voltammetry and 0.3 M for electrolysis experiments. Concentrations in the range $1.1–1.3 \times 10^{-3}$ M were used for the complexes studied. All experiments were carried out at 25 °C in the absence of oxygen. Dry nitrogen was bubbled through the solution in the cell before measurements.

Cyclic Voltammetry Simulation: Digital simulation of cyclic voltammograms was carried out using a custom-made program, developed in Turbo Pascal 6 (© Borland Inc.) and run on a Pentium IV computer at 2.4 GHz. The solution of the partial differential equations describing the reaction ion-diffusion processes of all the species involved in the mechanism was performed by the method of lines, using a non-uniform space grid.[52] Space discretisation was performed upon a diffusion layer (δ) computed according to the formula $\partial = \sqrt{(\pi D\tau)}$, where D is the diffusion coefficient and τ is the duration of each scan.[53] The time-course integration of the differential equations resulting from the semi-discretisation process of the space coordinate was carried out using a fourth-order Runge–Kutte method. Parameter estimation was performed by visual fitting of simulated data to a series of base-line-corrected experimental voltammograms, using a single set of model parameters. In this procedure, the parameters involved in the model were systematically varied so as to obtain the best possible agreement between the simulated and the experimental values. Various mechanisms were tried, starting from a simple ECE scheme, which was refined so that the most relevant features of the voltammetric response were explained, resulting in the proposed scheme.

Controlled-Potential Coulometry: Digital simulation of the experiments was carried out in Excel (© Microsoft Corporation). The relevant differential equations were solved using the Euler method and the parameters were estimated by least-squares regression using the Solver utility to minimize the sum of the square of the residuals.

Supporting Information (see footnote on the first page of this article): Voltammograms of **5** in different solvents (thf, CH_2Cl_2 and CH_3CN) at different scan rates and with Bu_4NBF_4 or Bu_4NPF_6 as supporting electrolyte; graphics of current vs. time for controlled potential coulometry of **5**; simulation curves of CV and CPC results.

Acknowledgments

The authors would like to thank the Fundação para a Ciência e a Tecnologia, Portugal for funding this work (research project POCI/QUI/55744/2004 and research grant SFRH/BD/13374/2003).

---

[1] A. M. Martins, C. C. Romão, M. Abrantes, M. C. Azevedo, J. L. Cui, A. R. Dias, M. T. Duarte, M. A. Lemos, T. Lourenco, R. Poli, *Organometallics* **2005**, *24*, 2582–2589.

[2] A. M. Martins, R. Branquinho, J. L. Cui, A. R. Dias, M. T. Duarte, J. Fernandes, S. S. Rodrigues, *J. Organomet. Chem.* **2004**, *689*, 2368–2376.

[3] R. M. Bullock, M. H. Voges, *J. Am. Chem. Soc.* **2000**, *122*, 12594–12595.

[4] B. F. M. Kimmich, P. J. Fagan, E. Hauptman, W. J. Marshall, R. M. Bullock, *Organometallics* **2005**, *24*, 6220–6229.

[5] L. C. Song, L. Y. Zhang, Q. M. Hu, X. Y. Huang, *Inorg. Chim. Acta* **1995**, *230*, 127–131.

[6] R. D. Adams, F. A. Cotton, *Inorg. Chim. Acta* **1973**, *7*, 153–156.

[7] A. S. Goldman, D. R. Tyler, *J. Am. Chem. Soc.* **1986**, *108*, 89–94.

[8] R. D. Adams, M. Brice, F. A. Cotton, *J. Am. Chem. Soc.* **1973**, *95*, 6594–6602.

[9] A. L. Rheingol, J. Harper, *Acta Crystallogr., Sect. C* **1991**, *47*, 184–186.

[10] R. B. King, M. B. Bisnette, *J. Organomet. Chem.* **1967**, *8*, 287–297.

[11] M. Cousins, M. L. H. Green, *J. Chem. Soc.* **1963**, 889.

[12] M. L. H. Green, A. N. Stear, *J. Organomet. Chem.* **1964**, *1*, 230–234.

[13] L.-C. Song, J.-Q. Wang, W.-J. Zhao, Q.-M. Hu, Y.-Q. Fang, S.-J. Zhang, R.-J. Wang, H.-G. Wang, *J. Organomet. Chem.* **1993**, *453*, 105–109.

[14] R. B. King, A. Fronzaglia, *Inorg. Chem.* **1966**, *5*, 1837–1846.

[15] S. P. Nolan, C. D. Hoff, J. T. Landrum, *J. Organomet. Chem.* **1985**, *282*, 357–362.

[16] R. D. Adams, D. M. Collins, F. A. Cotton, *Inorg. Chem.* **1974**, *13*, 1086–1090.

[17] A. Avey, S. C. Tenhaeff, T. J. R. Weakley, D. R. Tyler, *Organometallics* **1991**, *10*, 3607–3613.

[18] H. G. Alt, J. S. Han, R. D. Rogers, *J. Organomet. Chem.* **1993**, *454*, 165–172.

[19] T. J. R. Weakley, A. A. Avey Jr, D. R. Tyler, *Acta Crystallogr., Sect. C* **1992**, *48*, 154–155.

[20] H. Sitzmann, G. Wolmershauser, *Chem. Ber.* **1994**, *127*, 1335–1342.

[21] A. M. Martins, M. M. Marques, J. R. Ascenso, A. R. Dias, M. T. Duarte, A. C. Fernandes, S. Fernandes, M. J. Ferreira, I. Matos, M. C. Oliveira, S. S. Rodrigues, C. Wilson, *J. Organomet. Chem.* **2005**, *690*, 874–884.

[22] G. Huttner, H. H. Brintzinger, L. G. Bell, P. Friedrich, V. Bejenke, D. Neugebauer, *J. Organomet. Chem.* **1978**, *145*, 329–333.

[23] J. R. Ascenso, C. G. de Azevedo, I. S. Goncalves, E. Herdtweck, D. S. Moreno, M. Pessanha, C. C. Romão, *Organometallics* **1995**, *14*, 3901–3919.

[24] R. J. Klingler, W. M. Butler, M. D. Curtis, *J. Am. Chem. Soc.* **1978**, *100*, 5034–5039.

[25] J. Potenza, P. Giordano, D. Mastropa, A. Efraty, *Inorg. Chem.* **1974**, *13*, 2540–2544.

[26] M. D. Curtis, W. M. Butler, *J. Organomet. Chem.* **1978**, *155*, 131–145.

[27] M. A. Greaney, J. S. Merola, T. R. Halbert, *Organometallics* **1985**, *4*, 2057–2058.

[28] J. S. Huang, L. F. Dahl, *J. Organomet. Chem.* **1983**, *243*, 57–68.

[29] F. Shafiq, D. J. Szalda, C. Creutz, R. M. Bullock, *Organometallics* **2000**, *19*, 824–833.

[30] M. Calvo, P. Gomez-Sal, A. Manzanero, P. Royo, *Polyhedron* **1998**, *17*, 1081–1089.

[31] L. Brammer, D. Zhao, R. M. Bullock, R. K. Mcmullan, *Inorg. Chem.* **1993**, *32*, 4819–4824.

[32] P. Leoni, E. Grilli, M. Pasquali, M. Tomassini, *J. Chem. Soc., Dalton Trans.* **1986**, 1041–1043.

[33] R. J. Klingler, W. Butler, M. D. Curtis, *J. Am. Chem. Soc.* **1975**, *97*, 3535–3536.

[34] K. M. Kadish, D. A. Lacombe, J. E. Anderson, *Inorg. Chem.* **1986**, *25*, 2246–2250.

[35] M. Tilset, *Inorg. Chem.* **1994**, *33*, 3121–3126.

[36] J. R. Pugh, T. J. Meyer, *J. Am. Chem. Soc.* **1992**, *114*, 3784–3792.

[37] M. A. Alvarez, G. Garcia, M. E. Garcia, V. Riera, M. A. Ruiz, M. Lanfranchi, A. Tiripicchio, *Organometallics* **1999**, *18*, 4509–4517.

[38] T. Y. Cheng, B. S. Brunschwig, R. M. Bullock, *J. Am. Chem. Soc.* **1998**, *120*, 13121–13137.

[39] S. Namorado, J. R. Ascenso, A. M. Martins, unpublished work.

[40] M. F. N. N. Carvalho, M. A. N. D. A. Lemos, L. F. Veiros, G. R. Stephenson, *J. Organomet. Chem.* **2001**, *632*, 49–57.

[41] D. C. Barbini, P. S. Tanner, T. D. Francone, K. B. Furst, W. E. Jones, *Inorg. Chem.* **1996**, *35*, 4017–4022.

[42] K. M. Kadish, D. A. Lacombe, J. E. Anderson, *Inorg. Chem.* **1986**, *25*, 2246–2250.

[43] J. R. Pugh, T. J. Meyer, *J. Am. Chem. Soc.* **1992**, *114*, 3784–3792.

[44] A. Asdar, M. J. Tudoret, C. Lapinte, *J. Organomet. Chem.* **1988**, *349*, 353–366.

[45] M. L. Marcos, C. Moreno, R. M. Medina, M. J. Macazaga, S. Delgado, J. Gonzalez-Velasco, *J. Organomet. Chem.* **1998**, *568*, 185–196.

[46] R. Moulton, T. W. Weidman, K. P. C. Vollhardt, A. J. Bard, *Inorg. Chem.* **1986**, *25*, 1846–1851.

[47] G. M. Sheldrick, *SHELXL-97, A program for refining crystal structures*, University of Göttingen, Germany, **1998**.

[48] A. Altomare, M. C. Burla, M. Camalli, G. Cascarano, C. Giacovazzo, A. Guagliardi, A. G. G. Moliterni, G. Polidori, R. Sparna, *J. Appl. Crystallogr.* **1999**, *32*, 115–119.

[49] L. J. Farrugia, *J. Appl. Crystallogr.* **1999**, *32*, 837–838.
[50] L. J. Farrugia, *J. Appl. Crystallogr.* **1997**, *30*, 565.
[51] G. Gritzner, J. Kuta, *J. Electrochim. Acta* **1984**, *29*, 869–873.
[52] M. A. N. D. A. Lemos, A. J. L. Pombeiro, in *Molecular Electrochemistry of Inorganic, Bioinorganic and Organometallic Compounds*, vol. 385 (Eds.: A. J. L. Pombeiro, J. A. McCleverty), Kluwer Academic Publishers, Dordrecht, **1993**, p. 477.
[53] D. Britz, *Digital Simulation in Electrochemistry*, 2nd ed., Springer-Verlag, Berlin, **1988**.

Received: August 21, 2006